LETTERS
PUBLISHED ONLINE: 11 APRIL 2016 | DOI: 10.1038/NCLIMATE2987
nature climate change

Future freshwater stress for island populations

Kristopher B. Karnauskas[1,2*], Jeffrey P. Donnelly[3] and Kevin J. Anchukaitis[4]

Global climate models project large changes in the terrestrial water balance for many regions over this century in response to greenhouse gas emission[1–9], but insufficient resolution precludes such knowledge for approximately 18 million people living on small islands scattered across the world ocean. By accounting for evaporative demand a posteriori at 80 island groups distributed among Earth's major ocean basins, we reveal a robust yet spatially variable tendency towards increasing aridity at over 73% of island groups (16 million people) by mid-century. Although about half of the island groups are projected to experience increased rainfall—predominantly in the deep tropics—projected changes in evaporation are more uniform, shifting the global distribution of changes in island freshwater balance towards greater aridity. In many cases, the magnitude of projected drying is comparable to the amplitude of the estimated observed interannual variability, with important consequences for extreme events as well as mean climate. Future freshwater stress, including geographic and seasonal variability, has important implications for climate change adaptation scenarios for vulnerable human populations living on islands across the world ocean.

Within the expanse of the global ocean live tens of millions of people on thousands of islands much smaller than the grid resolution of current-generation global climate models (GCMs). The UN estimated the total population of Small Island Developing States to be 64 million in 2010, expecting to rise to 80 million by 2100. Island nations contribute a negligible quantity to global anthropogenic forcing relative to their population and vulnerability[10–12], but computational limitations preclude their representation in GCMs and exacerbate this social inequality[13,14]. Freshwater stress resulting from anthropogenic climate change may compound other water-related issues faced by geographically small island nations, such as population growth[15] and inundation due to sea-level rise[16]. Thus, a comprehensive assessment of the likely future changes in the freshwater balance, including their uncertainty, is critical for adaptation planning and freshwater management[17].

The sub-grid-scale islands and atolls of the world can be grouped into 80 politically or geographically distinct island groups, which include many independent, sovereign nations as well as territories of larger countries that are otherwise represented in GCMs (Table 1). The median size of an atmosphere/land grid cell in the Coupled Model Intercomparison Project Phase 5 (CMIP5)[18] is 2.5° longitude by 1.9° latitude (or 240 km by 210 km at 30° N), which is three times the combined land area of the Hawaiian Islands. High-resolution regional downscaling projects (for example, CORDEX; ref. 19) resolve down to 0.44° , which is sufficient to fit ∼5 grid cells into Hawaii (Big Island). Islands in such groups as French Polynesia, the Marshall Islands, and the Lesser Antilles—home to some of the most water vulnerable societies on the planet[20–22]—simply do not exist in today's GCMs.

A comprehensive assessment of freshwater resource availability demands perspective beyond rainfall projections. To account for the influence of surface processes, the difference between precipitation and evaporation ($P-E$) is often used to characterize the surface freshwater balance[1], or the ratio of precipitation to potential evapotranspiration (P/PE) as a measure of aridity[23]. However, GCM-derived evaporation from the ocean surface cannot be substituted for terrestrial potential evapotranspiration (PE) as it is dominated by a different mix of physical processes and can be an order of magnitude larger than over land. Therefore, the only component of the freshwater balance diagnosed by GCMs for sub-grid-scale islands is precipitation. Given the well-known influence of surface air temperature and other parameters on PE, and projected increases in surface air temperature for the 80 islands and island groups catalogued here ranging between $1.8\pm0.5\,^{\circ}C$ and $3.7\pm0.8\,^{\circ}C$ by 2090 under RCP8.5 forcing (multi-model mean $\pm$ 1 s.d. of the inter-model spread, for the two island groups among those catalogued here with the minimum and maximum multi-model mean projected warming), GCM experiments and the Intergovernmental Panel on Climate Change (IPCC) Assessment Reports that draw from them leave ∼18 million of the most vulnerable global population with incomplete projections of future stress on freshwater resources.

The barrier to evaluating future changes in freshwater availability on sub-grid-scale islands is that evaporation (or PE) is not specified for them in GCMs. However, it is possible to estimate terrestrial PE on an island that is missing from these models by assuming the near-surface climate on such an island is similar to that of the surrounding area (order ∼100 km scale). Then, PE can be calculated using an appropriate method based on near-surface climatic variables, supplying those inputs from the GCM experiments at the geographic locations where islands ought to be. One can imagine the suitability of this approximation varying from island to island—and with distance from shore—according to such physical characteristics as area or elevation, ranging from low-lying coral atolls such as the Maldives to the interior of volcanic islands such as Fiji. Prominent orography creates complex rainfall patterns and microclimates around islands through interaction with the trade winds, but the overall supply of moisture for precipitation and average regional temperatures driving evaporation are fundamentally linked to the large-scale circulation and energy balance, which are valid with or without an island. The observations provided in Supplementary Figs 1 and 2 explicitly demonstrate the validity of this approximation at two distinct island settings—Kwajalein Atoll and the Hawaiian Islands. Despite mean offsets among the various Hawaiian Islands of ∼1 °C relative to an offshore mooring, the seasonal and interannual

[1]Cooperative Institute for Research in Environmental Sciences (CIRES), University of Colorado Boulder, 216 UCB, Boulder, Colorado 80309-0216, USA. [2]Department of Atmospheric and Oceanic Sciences, University of Colorado Boulder, 311 UCB, Boulder, Colorado 80309-0311, USA. [3]Department of Geology and Geophysics, Woods Hole Oceanographic Institution, 266 Woods Hole Road, Woods Hole, Massachusetts 02543-1050, USA. [4]School of Geography and Development, University of Arizona, PO Box 210137, Tucson, Arizona 85721, USA. *e-mail: kristopher.karnauskas@colorado.edu

Table 1 | Islands considered in this study.

Ocean (and islands)	Lat.	Lon.	Pop. (k)
Pacific Ocean			
Ryukyu Islands	26° N	128° E	1,550
Hawaii	21° N	158° W	1,420
Fiji	18° S	179° E	858
Solomon Islands	9° S	160° E	523
French Polynesia			
Society Islands	17° S	151° W	235
Tuamotus	17° S	143° W	18
Marquesas Islands	9° S	140° W	9
Austral Islands	24° S	149° W	7
Gambier Islands	22° S	136° W	2
New Caledonia	21° S	165° E	269
Vanuatu	18° S	168° E	267
Samoa	14° S	172° W	179
Guam	13° N	145° E	159
Fed. Micronesia	7° N	152° E	106
Tonga	21° S	175° W	103
Republic of Kiribati			
Gilbert Islands	0° N	174° E	93
Teraina/Tabuaeran/Kiritimati	3° N	158° W	9
Banaba	1° S	170° E	≤1
Phoenix Islands	3° S	172° W	≤1
Starbuck/Malden	5° S	155° W	≤1
Vostok/Caroline/Flint	10° S	151° W	≤1
Marshall Islands	8° N	168° E	68
American Samoa	14° S	171° W	56
N. Mariana Islands	17° N	146° E	54
Galapagos	0° N	91° W	27
Palau	7° N	134° E	21
Cook Islands			
Southern Cook Islands	21° S	160° W	13
Northern Cook Islands	11° S	161° W	7
Wallis and Futuna	13° S	176° W	16
Tuvalu	9° S	179° E	11
Nauru	1° S	167° E	9
Easter Island	27° S	109° W	6
Ogasawara/Kazan Islands	26° N	142° E	3
Norfolk Island	29° S	168° E	2
Niue	19° S	170° W	2
Tokelau	9° S	172° W	≤1
J. Fernandez Islands	34° S	79° W	≤1
Chatham Islands	44° S	176° W	≤1
Lord Howe Island	32° S	159° E	≤1
Pitcairn Islands	25° S	130° W	≤1
Socorro Island	19° N	111° W	≤1
Guadalupe Island	29° N	118° W	≤1
Raoul/Macauley/Cheeseman	30° S	178° W	≤1
Minami-Tori-Shima	24° N	154° E	≤1
Pacific Ocean (cont'd)			
Coral Sea Islands	16° S	150° E	≤1
Cocos Island	6° N	87° W	≤1
Clipperton Island	10° N	109° W	≤1
San Felix	26° S	80° W	≤1
US Minor Outlying Islands			
Midway Atoll	28° N	177° W	≤1
Wake Atoll	19° N	167° E	≤1
Johnston Atoll	17° N	170° W	≤1
Palmyra Atoll	6° N	162° W	≤1
Howland/Baker	0° N	176° W	≤1
Jarvis Island	0° N	160° W	≤1
			6,102
Atlantic Ocean			
Lesser Antilles	15° N	61° W	3,736
Canary Islands	28° N	17° W	2,118
Cape Verde	15° N	24° W	512
Bahamas	25° N	77° W	319
Madeira	33° N	17° W	268
Azores	38° N	26° W	246
São Tomé & Príncipe	0° N	7° E	187
Bermuda	32° N	65° W	64
St Helena, Ascension & Tristan da Cunha			
Saint Helena	16° S	6° W	4
Ascension Island	8° S	14° W	≤1
Tristan da Cunha	37° S	12° W	≤1
Fernando de Noronha	4° S	32° W	3
Trindade Island	21° S	29° W	≤1
			7,457
Indian Ocean			
Mauritius	20° S	58° E	1,261
Reunion	21° S	56° E	841
Comoros	12° S	43° E	798
Andaman & Nicobar	12° N	93° E	381
Maldives	4° N	73° E	341
Mayotte	13° S	45° E	213
Seychelles	5° S	55° E	90
Lakshadweep	11° N	73° E	64
Minicoy	8° N	73° E	9
Chagos Islands	7° S	72° E	4
Christmas Island	11° S	106° E	2
Amsterdam/St Paul	38° S	78° E	≤1
Cocos Islands	12° S	97° E	≤1
			4,004
Total population (thousands)			17,563

Latitude, longitude and population (thousands) of the 80 island groups considered in this study, sorted by basin and population. Here, for convenience, 'island groups' refer both to individual islands (either independent or part of a larger continental nation) as well as polities composed of many individual islands. The general criteria for inclusion is that it is small enough to be completely unresolved by the majority of GCMs (ruling out, for example, Madagascar and Cuba), yet far enough from a major (well resolved) continent that the continent itself cannot be a reliable proxy for the island (ruling out, for example, Nantucket and the 'ABC' islands of Aruba, Curaçao and Bonaire—officially part of the Lesser Antilles), and between 50° S and 50° N. Independent, sovereign nations (and the US Minor Outlying Islands) that have been separated into multiple island groups owing to significant distances (thus possibly differing climate projections) are indented beneath the name of the nation to which they belong.

variability of on-island air temperature is remarkably well correlated with the mooring (160 km away). Similarly, at Kwajalein, despite differences in the amplitude of the diurnal cycle, the day-to-day variability in air temperature, humidity, and even wind speed across the atoll is virtually indistinguishable from that measured by a mooring 310 km offshore. The extent to which the near-surface climate is modified by the presence of a partially resolved island (Viti Levu, Fiji) in one GCM[24] is demonstrated in Supplementary Fig. 3.

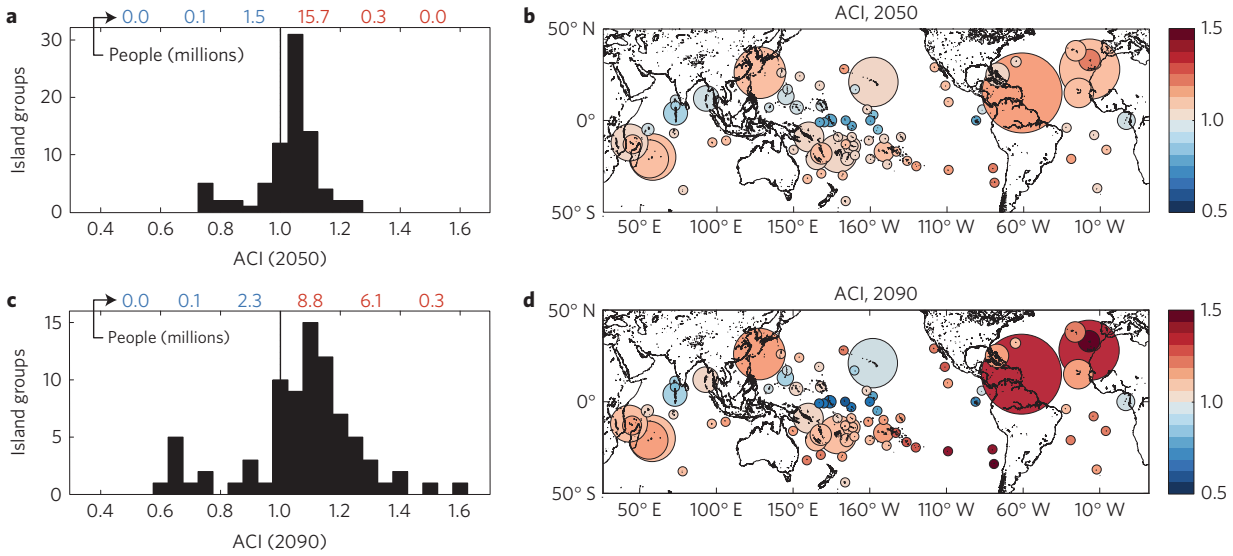

Figure 1 | Future aridity changes. a–d, Aridity change index (ACI) for 2050 (**a**,**b**) and 2090 (**c**,**d**) expressed as histograms (**a**,**c**) and bubble maps (**b**,**d**). The total number of people (in millions) in each bin is indicated at the top of each histogram. High-resolution coastline data are from the Global Self-consistent, Hierarchical, High-resolution Geography (GSHHG) database version 2.2.3[40]. In this figure, and all bubble maps, the area of each bubble is linearly proportional to the population represented. A minimum bubble size equivalent to a population of 50,000 people is enforced to ensure visibility.

The influence of the island on the simulated near-surface air temperature (T_a) and humidity (q_a) climatology is negligible, whereas there is a discernible signature in surface downwelling shortwave radiation (R_o) and precipitation (P); on average, the model island is slightly rainier than its immediate surroundings. In terms of the response of the local climate to radiative forcing, however, the influence of the island is clearly distinguishable only in ΔT_a, where there is a modest (<0.1°C) additional warming on top of the ~3 °C warming for the surrounding area. The latter is consistent with the fact that land surfaces typically warm faster than the ocean mixed layer in response to surface forcing, implying that the aforementioned approximation may lead to conservative estimates of increased PE if land surfaces indeed warm faster, but will ignore changes in orographic precipitation due to changes in trade wind strength or direction.

Among the methods to calculate PE, the Penman–Monteith method[25–27] is now widely used for studies of transient climate change[3,4], as it is physically based and does not overestimate the response of PE to temperature change, in contrast to others that are empirically calibrated to the present climate[28]. The UN Food and Agricultural Organization (FAO) Penman–Monteith method, originally developed for a well-watered reference crop surface, requires near-surface T_a, q_a, wind speed (u_2), and surface air pressure (p_s), as well as surface net radiation (R_n) and heat flux into the ground (G). Focusing exclusively on continental regions, several previous assessments of Penman–Monteith PE based on GCM simulations have exploited the equivalence of the radiative term ($R_n - G$) with the sum of latent (LH) and sensible (SH) heat fluxes, which are standard GCM outputs[3]. Because sub-grid-scale island surfaces in GCMs, by definition, behave as the open ocean, and LH and SH in this context are indeed strictly terrestrial in nature, here we explicitly compute R_n and G according to the recommended practice of the American Society of Civil Engineers[29], which relies only on near-surface climate parameters, thus eliminating the requirement that a land surface actually be present in the GCM. See Methods for more details on the Penman–Monteith method and its implementation in this study.

An aridity change index (ACI) is computed for each island group listed in Table 1, and for each CMIP5 GCM listed in Supplementary Table 1. Here we define ACI as the ratio of the fractional change in potential evaporation to the fractional change in precipitation: $\mathrm{ACI} = (PE_F/PE_H)/(P_F/P_H)$, where subscript F indicates future, and subscript H indicates historical. Here, future is defined as the mean climate over the period 2041–2059 ('2050') or 2081–2099 ('2090') in the Representative Concentration Pathway 8.5 (RCP8.5) scenario of the IPCC Fifth Assessment Report (AR5), whereas the historical period is defined as 1981–1999 in the corresponding historical experiments.

The resulting ACI projections for the world's sub-grid-scale islands in 2050 and 2090 are shown in Fig. 1. There is substantial geographic variability in ACI both at the middle and end of the twenty-first century, including increasingly wet conditions (ACI < 1) in the Maldives and islands along the equatorial Pacific such as the Gilberts (Republic of Kiribati). At least one island group in each ocean basin also shows no projected aridity change (ACI ≈ 1), either through compensating changes in P and PE, or no change in either. For the majority of island groups, however, there is a robust tendency towards increasing aridity; 73% of the island groups considered here are projected to exhibit drying conditions (ACI > 1) by 2050, with the mean and spread clearly shifting further towards aridification by 2090. In terms of population, 16.0 (15.2) million people, or 91% (86%) of the total population considered, are projected to experience increased aridity by 2050 (2090). Among the island groups with the most severe projected increases in aridity in 2090 are the Juan Fernandez 'Robinson Crusoe' Islands, Chile (ACI = 1.6), Easter Island, Chile (ACI = 1.4), the Lesser Antilles (ACI = 1.4), the Tuamotus, French Polynesia (ACI = 1.3), and the Azores (ACI = 1.2). The basin-scale patterns, particularly the higher ACI in the subtropics and increasingly towards the eastern boundaries, are qualitatively consistent with recently identified robust responses of the atmospheric general circulation and hydrologic cycle to radiative forcing[2,5,30–32]. Although the Greater Antilles (for example, Cuba and Hispaniola) are not included in our study, because they are large enough to be resolved by many of today's GCMs, they are home to nearly 40 million people, and recent studies analysing future hydroclimate changes on well-resolved landmasses project that the Greater Antilles will experience drying similar to that shown here for the Lesser Antilles[4,7].

ACI projections are also fairly robust across the 22 GCMs analysed, with inter-model standard deviations in the range

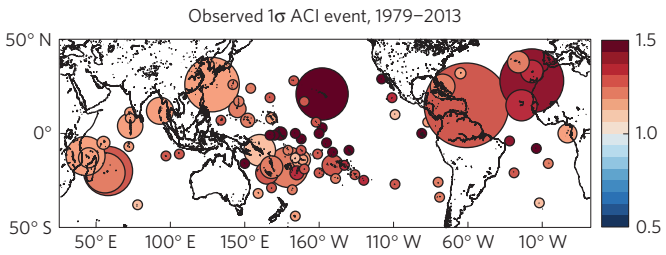

Figure 2 | Internal variability of aridity. Estimated observed magnitude of a local 1σ positive (dry) ACI event, defined as 1 + the local temporal standard deviation of ACI (annually smoothed). Precipitation data are from the Global Precipitation Climatology Project (GPCP) v2.2[33] and *PE* is calculated from NCEP/NCAR Reanalysis fields[34].

~0.1–0.2 in 2050, ~0.2–0.3 in 2090, and generally scaling proportional to ACI magnitudes (Supplementary Figs 4–5). The local, relative importance of the projected changes shown in Fig. 1 can be judged by comparing them to the amplitude of year-to-year variability experienced at each island group over the past 35 years based on *P* measured by satellite[33] combined with *PE* calculated from reanalysis fields[34] (Fig. 2). The largest amplitude ACI variability, in terms of the magnitude of a local 1σ positive (dry) ACI event, is found in the equatorial Pacific, which is unsurprising given the influence of the El Niño–Southern Oscillation (ENSO) on rainfall and most other climatic variables[35,36]. Elsewhere, ACI interannual standard deviations are in the range ~0.1–0.3. Thus, the ACI projections shown in Fig. 1 in terms of changes in mean climate are equivalent to ~80–100% of the local amplitude of interannual variability. Therefore, the projected changes in mean climate will impose a direct stress on freshwater resources for many societies across the global ocean, while shifting the baseline on which natural variations will superimpose.

The seasonal cycle of changes in *P* and *PE* also varies considerably among island groups, as illustrated by six examples for island groups with annual ACI ranging from <1 (Maldives) to near 1 (Marshall Islands) to increasingly higher ACI (Easter Island) (Fig. 3). In all cases, the seasonal cycle of rainfall trends dictate the seasonality of ACI, whereas there is much smaller seasonal variation in the long-term *PE* change. At the Marshall Islands, increased aridity is expected in boreal spring, with decreased aridity in summer, effectively cancelling over the annual cycle. At Easter Island, where the projected annual mean ACI is fairly high (ACI = 1.4), ACI up to 1.6 is expected in austral summer, owing to the seasonally dependent trends in *P* and *PE* being in phase. Partitioning of the effects of changes in *PE* and *P* leading to the overall ACI across all 80 sites (Fig. 4) reveals that the change in *PE* always contributes to higher ACI (~1.1), which further compounds reduced *P* at some island groups (for example, Mauritius) and at least partially offsets increased *P* at others (for example, the Maldives). Without accounting for projected changes in *PE*, that is, based on *P* alone, the 80 island groups considered here would be approximately evenly split into wetter or drier categories by 2090.

Considerable effort across several disciplines has led to detailed characterizations of the global water cycle and its response to radiative forcing, from the landmasses large enough to be well resolved by state-of-the-art GCMs[1,3,4,7–9] to the other ~71% of the planet covered by open ocean[30,37,38]. Meanwhile, ~18 million people, many of whom live with acute vulnerability to exacerbated freshwater stress combined with additional water-related issues, despite accounting for negligible greenhouse gas emissions, have fallen through the cracks—the computationally disenfranchised. By moving beyond rainfall projections and accounting for changes in the climate system's evaporative demand for water, the picture of future freshwater stress that emerges is variable from one island group to another, but with a clear trajectory for the majority of islands towards a more arid climate—similar to recent continental studies[4,39]. Further, the strong seasonal

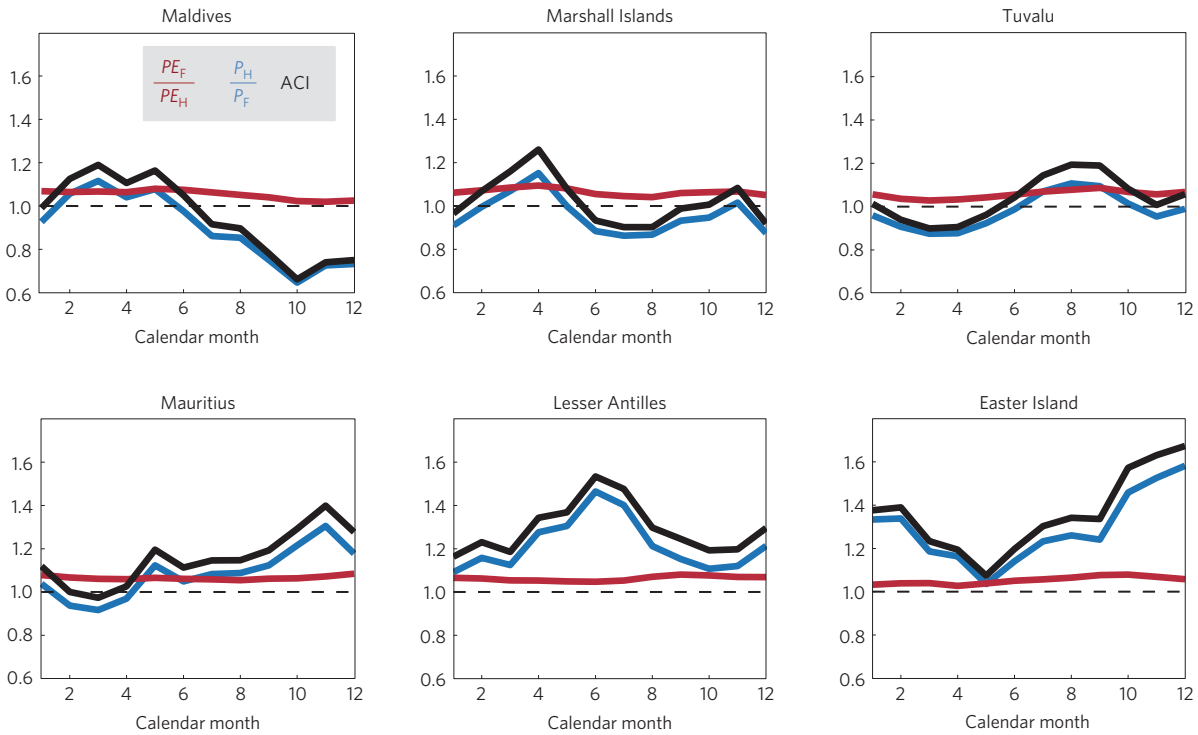

Figure 3 | Seasonal changes in aridity. Seasonal cycle of changes in ACI for 2090 including the contributions of changes in *PE* and changes in *P* at six select island groups.

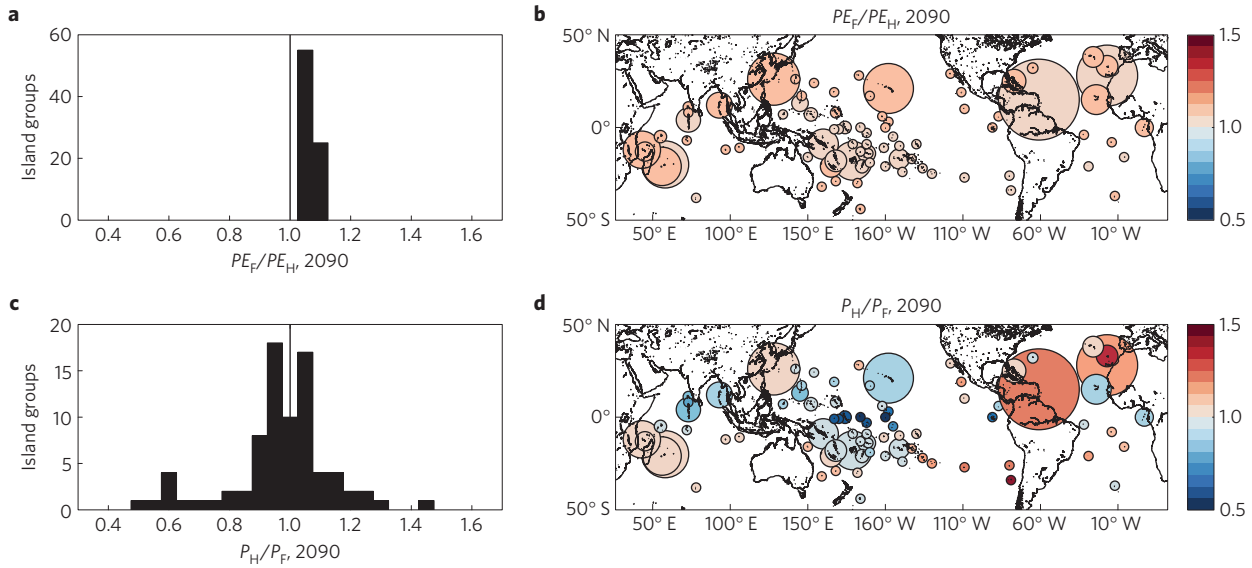

Figure 4 | Effects of precipitation and evaporation. a–d, Partitioning of ACI in 2090 between the contributions of changes in *PE* (**a**,**b**) and changes in *P* (**c**,**d**) expressed as histograms (**a**,**c**) and bubble maps (**b**,**d**).

dependence of future freshwater stress has important, actionable implications for adaptation of freshwater management practices in a changing climate[17].

Methods

Methods and any associated references are available in the online version of the paper.

Received 11 March 2015; accepted 3 March 2016; published online 11 April 2016

References

1. Laine, A., Nakamura, H., Nishii, K. & Miyasaka, T. A diagnostic study of future evaporation changes projected in CMIP5 climate models. *Clim. Dynam.* **42,** 2745–2761 (2014).
2. Scheff, J. & Frierson, D. Twenty-first-century multimodel subtropical precipitation declines are mostly midlatitude shifts. *J. Clim.* **25,** 4330–4347 (2012).
3. Scheff, J. & Frierson, D. M. W. Scaling potential evapotranspiration with greenhouse warming. *J. Clim.* **27,** 1539–1558 (2014).
4. Cook, B. I., Smerdon, J. E., Seager, R. & Coats, S. Global warming and 21st century drying. *Clim. Dynam.* **43,** 2607–2627 (2014).
5. Huang, P., Xie, S. P., Hu, K. M., Huang, G. & Huang, R. H. Patterns of the seasonal response of tropical rainfall to global warming. *Nature Geosci.* **6,** 357–361 (2013).
6. Rotstayn, L. D. *et al*. Aerosol- and greenhouse gas-induced changes in summer rainfall and circulation in the Australasian region: a study using single-forcing climate simulations. *Atmos. Chem. Phys.* **12,** 6377–6404 (2012).
7. Dai, A. G. Increasing drought under global warming in observations and models. *Nature Clim. Change* **3,** 52–58 (2013).
8. Huang, J., Yu, H., Guan, X., Wang, G. & Guo, R. Accelerated dryland expansion under climate change. *Nature Clim. Change* **6,** 166–171 (2016).
9. Chadwick, R., Good, P., Martin, G. & Rowell, D. P. Large rainfall changes consistently projected over substantial areas of tropical land. *Nature Clim. Change* **6,** 177–181 (2016).
10. Hay, J. E. & Sem, G. *GHG Inventories in PICCAP Countries: Evaluation and Regional Synthesis of National Greenhouse Gas Inventories: General Assessment and Regional Synthesis* (South Pacific Regional Environment Programme, 2000).
11. Barnett, J. Adapting to climate change in Pacific Island Countries: the problem of uncertainty. *World Dev.* **29,** 977–993 (2001).
12. IPCC *Climate Change 2014: Impacts, Adaptation, and Vulnerability* (eds Barros, V. R. *et al*.) (Cambridge Univ. Press, 2014).
13. Barnett, J., Lambert, S. & Fry, I. The hazards of indicators: insights from the environmental vulnerability index. *Ann. Assoc. Am. Geogr.* **98,** 102–119 (2008).
14. Vorosmarty, C. J., Green, P., Salisbury, J. & Lammers, R. B. Global water resources: vulnerability from climate change and population growth. *Science* **289,** 284–288 (2000).
15. United Nations Department of Economic and Social Affairs Population Division. *World Population Prospects: The 2012 Revision Special Aggregates.* ST/ESA/SER.A/335 (United Nations Department of Economic and Social Affairs Population Division, 2013).
16. Nicholls, R. J. & Cazenave, A. Sea-level rise and its impact on coastal zones. *Science* **328,** 1517–1520 (2010).
17. Mekonnen, M. M. & Hoekstra, A. Y. Four billion people facing severe water scarcity. *Sci. Adv.* **2,** e1500323 (2016).
18. Taylor, K. E., Stouffer, R. J. & Meehl, G. A. An overview of CMIP5 and the experiment design. *Bull. Am. Meteorol. Soc.* **93,** 485–498 (2012).
19. Jones, C., Giorgi, F. & Asrar, G. *The Coordinated Regional Downscaling Experiment: CORDEX; An International Downscaling Link to CMIP5* (International CLIVAR Project Office, 2011).
20. World Water Assessment Programme *Water for People, Water for Life: A Joint Report by the Twenty Three UN Agencies Concerned with Freshwater* (UNESCO, 2003).
21. Pacific Islands Forum Secretariat *Pacific Cooperation Plan: Preliminary Sector Analysis for Water, Sanitation and Hygiene* (South Pacific Applied Geoscience Commision, 2005); http://www.pacificwater.org/userfiles/file/Pacific%20Cooperation%20Plan%20-%20Preliminary%20Sector.pdf
22. Gassert, F., Reig, P., Luo, T. & Maddocks, A. *Aqueduct Country and River Basin Rankings: A Weighted Aggregation of Spatially Distinct Hydrological Indicators* 28 (World Resources Institute, 2013).
23. United Nations Environment Programme (Edward Arnold, 1992).
24. Hurrell, J. W. *et al*. The Community Earth System Model: a framework for collaborative research. *Bull. Am. Meteorol. Soc.* **94,** 1339–1360 (2013).
25. Penman, H. L. Natural evaporation from open water, hare soil and grass. *Proc. R. Soc. Lond. A* **193,** 120–145 (1948).
26. Monteith, J. L. Evaporation and surface-temperature. *Q. J. R. Meteorol. Soc.* **107,** 1–27 (1981).
27. Monteith, J. L. Evaporation and environment. *Symp. Soc. Exp. Biol.* **19,** 205–234 (1964).
28. Sheffield, J., Wood, E. F. & Roderick, M. L. Little change in global drought over the past 60 years. *Nature* **491,** 435–438 (2012).
29. Allen, R. G. *et al*. *The ASCE Standardized Reference Evapotranspiration Equation* (American Society of Civil Engineers, 2005).
30. Held, I. M. & Soden, B. J. Robust responses of the hydrological cycle to global warming. *J. Clim.* **19,** 5686–5699 (2006).
31. Vecchi, G. A. & Soden, B. J. Global warming and the weakening of the tropical circulation. *J. Climate* **20,** 4316–4340 (2007).
32. Lu, J., Vecchi, G. A. & Reichler, T. Expansion of the Hadley cell under global warming. *Geophys. Res. Lett.* **34,** L06805 (2007).
33. Adler, R. F. *et al*. The version-2 Global Precipitation Climatology Project (GPCP) monthly precipitation analysis (1979–present). *J. Hydrometeorol.* **4,** 1147–1167 (2003).

34. Kalnay, E. *et al*. The NCEP/NCAR 40-year reanalysis project. *Bull. Am. Meteorol. Soc.* **77,** 437–471 (1996).
35. Ropelewski, C. F. & Halpert, M. S. Global and regional scale precipitation patterns associated with the El-Niño Southern Oscillation. *Mon. Weath. Rev.* **115,** 1606–1626 (1987).
36. Meehl, G. A. Vulnerability of freshwater resources to climate change in the tropical Pacific region. *Water Air Soil Pollut.* **92,** 203–213 (1996).
37. Schmitt, R. W. The ocean component of the global water cycle. *Rev. Geophys.* **33,** 1395–1409 (1995).
38. Durack, P. J., Wijffels, S. E. & Matear, R. J. Ocean salinities reveal strong global water cycle intensification during 1950 to 2000. *Science* **336,** 455–458 (2012).
39. Scheff, J. & Frierson, D. M. W. Terrestrial aridity and its response to greenhouse warming across CMIP5 climate models. *J. Clim.* **28,** 5583–5600 (2015).
40. Wessel, P. & Smith, W. H. F. A global, self-consistent, hierarchical, high-resolution shoreline database. *J. Geophys. Res.* **101,** 8741–8743 (1996).

Acknowledgements

K.B.K. and J.P.D. acknowledge support from the Strategic Environmental Research and Development Program (SERDP). SERDP is the environmental science and technology programme of the US Department of Defense (DoD) in partnership with the US Department of Energy (DOE) and the US Environmental Protection Agency (EPA). K.B.K. further acknowledges support from the Alfred P. Sloan Foundation and the James E. and Barbara V. Moltz Fellowship administered by the WHOI Ocean and Climate Change Institute (OCCI). K.J.A. acknowledges support from NSF grant BCS–1263609. The authors thank C. Ummenhofer for helpful discussions. The authors thank NOAA NCDC for providing GHCN station observations. The WHOI—Hawaii Ocean Timeseries Site (WHOTS) mooring is supported by NOAA through the Cooperative Institute for Climate and Ocean Research (CICOR) under Grant No. NA17RJ1223 and NA090AR4320129 to WHOI, and by NSF grants OCE–0327513, OCE–752606, and OCE–0926766 to the University of Hawaii.

Author contributions

K.B.K. designed the study with substantial contributions from J.P.D. and K.J.A., K.B.K. analysed the data, all authors discussed and interpreted the results, K.B.K. wrote the initial draft of the manuscript, and all authors discussed and interpreted the results and edited the manuscript.

Additional information

Supplementary information is available in the online version of the paper. Reprints and permissions information is available online at www.nature.com/reprints. All data analysed in this study are publicly available. Correspondence and requests for materials should be addressed to K.B.K.

Competing financial interests

The authors declare no competing financial interests.

Methods

Calculating Potential Evapotranspiration on sub-grid-scale islands. Here we describe the calculation of Penman–Monteith Potential Evapotranspiration on sub-grid-scale islands using global climate models and reanalysis data. The Penman–Monteith method of calculating potential evapotranspiration (*PE*) is a solution to a system of equations describing the surface energy balance derived from near-surface climatic parameters. A common motivation for such an approach is to circumvent the paucity of direct measurements, and the difficulty in making them. Knowledge of *PE* is necessary so that the evaporative demand and its response to radiative forcing may be compared with that of precipitation (*P*), and aridity changes may be evaluated for small island climates. *PE* may be described simply as the rate of evaporation that would occur given an unlimited supply of water available to be evaporated. Although the ocean is effectively such a supply, the physics governing the rate of evaporation from an open ocean surface is different from that governing evaporation from land. This fact, and by extension the necessity to compute *PE* separately, is evident in a direct comparison between *PE* and *E* at the 80 island groups considered in this study (Supplementary Fig. 6). Because only a few of the islands considered in this study are actually resolved by only a few global climate models (GCMs), *E* in this case is taken from each model's open ocean surface (where there are islands in the real world). Not only is the annual mean *E* systematically higher than *PE* at ~80% of the island groups, there is considerable spread between *E* and *PE* across the 80 island groups ($r^2 = 0.27$). More importantly, the changes in *PE* (either fractional or difference) are essentially uncorrelated from those of *E* ($r^2 < 0.1$).

For a derivation and excellent discussion of the Penman–Monteith equation, the reader is referred to Scheff and Frierson[3], further details by the American Society of Civil Engineers (ASCE)[29], and the seminal papers by Penman and Monteith themselves[25,26]. The Penman–Monteith equation is given by:

$$\mathrm{PE} = \frac{C_0 \Delta (R_n - G) + \gamma C_n / (T_a + C_T) u_2 (e_s - e_a)}{\Delta + \gamma (1 + C_d u_2)}$$

where *PE* is potential evapotranspiration (mm d^{-1}), C_0 is a collection of coefficients (0.408 m^2 mm MJ^{-1}), Δ is the slope of the saturation vapour pressure as a function of temperature $e_s(T_a)$ curve (kPa °C^{-1}), R_n is the net downwelling radiation at the surface (MJ m^{-2} d^{-1}), *G* is the heat flux into the ground (MJ m^{-2} d^{-1}), γ is the psychrometric constant (kPa °C^{-1}), C_n is the numerator constant (900 K mm s^3 Mg^{-1} d^{-1}), T_a is the air temperature at 2 m (°C), C_T is the conversion from centigrade to kelvin (273 °C), u_2 is the wind speed at 2 m (m s^{-1}), e_s is the saturation vapour pressure at 2 m (kPa), e_a is the actual vapour pressure at 2 m (kPa), and C_d is the denominator constant (0.34 s m^{-1}). The slope of the saturation vapour pressure as a function of temperature Δ is calculated as $\Delta(T_a) = 2{,}503 \exp(17.27 T_a/(T_a + 237.3))/(T_a + 237.3)$ (ref. 2), the psychrometric 'constant' γ is calculated as $\gamma(p_s) = 0.000665 p_s$ where p_s is surface air pressure, saturation vapour pressure e_s is calculated as $e_s(T_a) = 0.6108 \exp(17.27 T_a/(T_a + 237.3))$, and the actual vapour pressure e_a is calculated as $e_a = q_a p_s/\varepsilon$ where q_a is specific humidity at 2 m and $\varepsilon = 0.622$.

Our calculation of almost every term in the equation for *PE* above closely follows previous investigations[3,4], which follow the detailed ASCE recommendations[29]. However, because we are calculating *PE* at locations where there is no land present in the GCMs, we cannot exploit the equivalence of the radiative term $(R_n - G)$ with the sum of latent (LH) and sensible (SH) heat fluxes and simply replace $(R_n - G)$ with LH + SH, as others have while focusing on landforms resolved by GCMs such as continents. Therefore, following ASCE[29], we compute net radiation at the surface R_n directly as $R_n = R_{ns} - R_{nl}$ where R_{ns} is the net shortwave radiation and R_{nl} is the net longwave radiation. We compute these terms as $R_{ns} = (1 - \alpha) R_s$, where $\alpha = 0.23$ (albedo for the standardized reference surface) and R_s is downwelling shortwave radiation, and $R_{nl} = \sigma f_{cd} (0.34 - 0.14\sqrt{e_a})\, T_a^4$, where σ is the Stefan–Boltzmann constant and $f_{cd} = 1.35 R_s/R_{so} - 0.35$ is the cloudiness function (where R_{so} is clear-sky shortwave radiation). Substantial differences between ocean and land emissivity are one reason why we elect to use the ASCE formulae rather than radiative fields simulated by the GCMs in open ocean grid cells. Also following ASCE[29], we compute the heat flux into the ground *G* as $G(i) = 0.07\,(T_a(i+1) - T_a(i-1))$, where *i* is the monthly increment.

Thus, our calculation of *PE* requires each of the following six GCM outputs: near-surface air temperature (CMIP5 variable *tas*), near-surface specific humidity (*huss*), near-surface wind speed (*sfcWind*), surface air pressure (*ps*), surface downwelling shortwave radiation (*rsds*), and surface downwelling clear-sky shortwave radiation (*rsdscs*). The Coupled Model Intercomparison Project-Phase 5 (CMIP5) GCMs listed in Supplementary Table 1 provided all of the required outputs for both the historical and RCP8.5 experiments and were thus included in this study on that basis. The outputs from each model were linearly interpolated to a common 1° by 1° grid to enable, for example, the calculation of multi-model mean results.

We also calculate Penman–Monteith *PE* using reanalysis data (Fig. 2), based on the National Centers for Environmental Prediction/National Center for Atmospheric Research (NCEP/NCAR) atmospheric reanalysis[34] over the time period 1979 through 2013. We do not compute *PE* before 1979, because the satellite precipitation measurements (Global Precipitation Climatology Project; GPCP) began in 1979. The computational procedures carried out using reanalysis data were identical to those applied to CMIP5 GCM output. The variables T_a, q_a, u_2, p_s, R_s, and R_{so} are provided directly from the reanalysis (http://www.esrl.noaa.gov/psd/data/gridded/data.ncep.reanalysis.html). The NCEP/NCAR reanalysis data and GPCP precipitation estimates were also linearly regridded onto the same 1° by 1° grid as in the GCM output.

References

41. Bi, D. H. *et al*. The ACCESS coupled model: description, control climate and evaluation. *Aust. Meteorol. Oceanogr.* **63,** 41–64 (2013).
42. Wu, T. W. *et al*. An overview of BCC climate system model development and application for climate change studies. *J. Meteorol. R.* **28,** 34–56 (2014).
43. Voldoire, A. *et al*. The CNRM-CM5.1 global climate model: description and basic evaluation. *Clim. Dynam.* **40,** 2091–2121 (2013).
44. Donner, L. J. *et al*. The dynamical core, physical parameterizations, and basic simulation characteristics of the atmospheric component AM3 of the GFDL global coupled model CM3. *J. Clim.* **24,** 3484–3519 (2011).
45. Dunne, J. P. *et al*. GFDL's ESM2 global coupled climate-carbon earth system models. Part II: carbon system formulation and baseline simulation characteristics. *J. Clim.* **26,** 2247–2267 (2013).
46. Schmidt, G. A. *et al*. Present-day atmospheric simulations using GISS ModelE: Comparison to *in situ*, satellite, and reanalysis data. *J. Clim.* **19,** 153–192 (2006).
47. Collins, W. J. *et al*. Development and evaluation of an Earth-System model-HadGEM2. *Geosci. Model Dev.* **4,** 1051–1075 (2011).
48. Volodin, E. M., Dianskii, N. A. & Gusev, A. V. Simulating present-day climate with the INMCM4.0 coupled model of the atmospheric and oceanic general circulations. *Izv. Atmos. Ocean. Phys.* **46,** 414–431 (2010).
49. Dufresne, J. L. *et al*. Climate change projections using the IPSL-CM5 Earth System Model: from CMIP3 to CMIP5. *Clim. Dynam.* **40,** 2123–2165 (2013).
50. Watanabe, S. *et al*. MIROC-ESM 2010: model description and basic results of CMIP5-20c3m experiments. *Geosci. Model Dev.* **4,** 845–872 (2011).
51. Watanabe, M. *et al*. Improved climate simulation by MIROC5. Mean states, variability, and climate sensitivity. *J. Clim.* **23,** 6312–6335 (2010).
52. Yukimoto, S. *et al*. A new global climate model of the meteorological research institute: MRI-CGCM3-model description and basic performance. *J. Meteorol. Soc. Jpn* **90,** 23–64 (2012).